Bull. Mater. Sci. (2022)45:154
https://doi.org/10.1007/s12034-022-02732-2

Fabrication and characterization of sol–gel-based coatings on quartz glass to obtain antireflective effect at 1054 nm for optics of high power Nd:phosphate glass laser

SUSMITA PODDER[1], APARAJITA MALLICK NATH[1], C MUKHERJEE[2,3], V V V SUBRAHMANYAM[4] and SUNIRMAL JANA[1,*]

[1]Specialty Glass Division, CSIR-Central Glass and Ceramic Research Institute, Kolkata 700032, India
[2]Laser Technology Division, Raja Ramanna Centre for Advanced Technology, Indore 452013, India
[3]Homi Bhabha National Institute, Training School Complex, Mumbai 400094, India
[4]Laser Technology Division, Raja Ramanna Centre for Advanced Technology, Indore 452013, India
*Author for correspondence (sjana@cgcri.res.in)

MS received 20 November 2021; accepted 15 April 2022

Abstract. In order to obtain higher laser-induced damage threshold (LIDT) and lower loss of laser radiation, the incident radiation must have an insignificant absorbance and high anti-reflectance. In this work, a single-layer porous SiO_2-based anti-reflective (AR) coating for the optics of Nd:phosphate laser system has been developed on quartz glass optics adopting sol–gel dip coating technique, following quarter wavelength optical design. As measured by spectroscopic ellipsometer, the refractive index (RI) of the coated layer is found to be ~1.2. A maximum transmittance of ~99% in single-layer-coated quartz glass has been achieved at 1054 nm. In addition, the non-quarter wavelength-based double layer with an optical design (glass/ 0.7153 M / 1.134 L / air) and triple-layer AR coating with an optical design (glass / 0.28 H / 1.65 M / 1.03 L / air, where H, M and L indicate one-quarter wave thick layers of high, medium and low RI materials) have been fabricated. The deposition of M and H layers has been made from mixed metal oxide precursor sols of zirconia-silica, while L has been made from silica precursor sol to obtain porous silica coating. A maximum transmittance of about 98.1 and 97.6% was found at 1054 nm in double- and triple-layer AR-coated samples, respectively. The LIDT values have been measured on the AR coatings. Based upon the number of layers in the AR coatings, the LIDT values varied in the range of 8.7–2.4 J cm^{-2} starting from single to double to triple layer. The AR coatings developed by sol–gel dip coating technique could find application in Nd:phosphate high power laser system.

Keywords. Sol–gel dip coating; dielectric metal oxide; multi-layer optical coating; anti-reflection coating; laser-induced damage threshold.

1. Introduction

Anti-reflection (AR) coating reduces a portion of light that reflects back from the surface of a substrate. Particularly for the optics used in laser construction, it is crucial to reduce the reflection for minimizing the loss of laser radiation [1]. Generally, the optical components of laser cavity especially in high power laser are coated with high-quality dielectric metal oxides to diminish the loss. Light reflection is an unwanted phenomenon in many optical instruments. Reflection from such surfaces causes loss of energy, thus, decreasing the efficiency of the optical instrument. When travelling from one medium to another, a change in refractive index (RI) at the interface causes light to reflect back from that surface. Researchers tried to modify the surface of the optical instrument by applying various techniques so that the change in RI is not abrupt [2]. Surface modifications including etching [3] or patterning of the surface [4–6] are made to avoid the sudden change in RI. Other than the above-mentioned methods, an AR coating could be applied onto the required surface to increase the transmission of light by reducing the RI.

Surface of quartz glass (RI = 1.46) normally transmits about 97% light in near-infrared region. This substrate is used (at lasing wavelength 1054 nm) to inhibit energy loss through radiation. AR coating is usually applied to amplify laser energy output of the laser source [7]. In this respect, the metal oxides such as SiO_2, ZrO_2, TiO_2, HfO_2, etc. [1,8] are used as optical materials that could able to withstand high power laser of GW range. Hence, these materials exhibit high laser-induced damage threshold (LIDT) value. The existence of any impurities and/or

Supplementary Information: The online version contains supplementary material at https://doi.org/10.1007/s12034-022-02732-2.

Published online: 04 August 2022

stress in the coating results in excessive absorption of high power energy and the coating could be damaged, consequently decreases the LIDT value [9]. Although, organic materials [10] and polymers [11,12] are some of the commonly used AR coating materials for the applications in high power laser, they are not suitable due to their tendency to absorb laser energy. In this regard, silica is vastly used as one of the AR coating materials for high damage resistance and transmittance [13]. On the other hand, sol–gel process is advantageous for the development of multi-component optical coatings compared to other conventional coating methods, such as magnetron sputtering [14,15], chemical vapor deposition [16,17], electron beam vapor deposition, pulsed laser deposition [18,19] and plasma-enhanced chemical vapor deposition [20–22]. However, these methods are very expensive for the production of larger-sized optics.

It is to be noted that sol–gel-based dip-coating technique is largely used to fabricate AR coatings for the application in high power laser performing at near-infrared region. In this regard, Zhang *et al* [23] prepared double-layered broadband AR silica coating with hydrophilic property showing 99.95 and 100% transmission at 532 and 1064 nm, respectively. Boron nitride sheet incorporated silica AR coating was also developed by Wang *et al* [13] and they showed 99.89% transmission and 10.98 J cm^{-2} LIDT value of the sample. Moreover, Ye *et al* [24] reported tri-wavelength broadband AR coatings using sol–gel-based silica thin films.

In this work, single-, double- and triple-layer AR coatings, namely 1LD, 2LD and 3LD, respectively, have been developed by a facile sol–gel dip-coating technique using easily available and non-expensive raw materials based on the quarter wavelength and non-quarter wavelength optical designs, respectively. The AR coatings on quartz glass have been developed for all three designs to obtain anti-reflection effect at 1054 nm. Silica and mixed silica-zirconia as the coating materials have been used. Single to multi-layer coating has been explored to get broad to narrow bandwidth. Also, the fabrication of single-layer AR coating with high mechanical strength is not possible because the low RI material is porous in nature. Hence, the multi-layer coatings become necessary. Sol–gel dip-coating technique was followed for the deposition of coating. A detailed study of the coatings has been done by using field emission scanning electron microscope (FESEM) and atomic force microscope (AFM) to understand the surface morphology of the coating layers. At 1054 nm, the percentage of transmittance has been achieved as high as 99% in case of single-layer silica coating and about 98.2% in multi-layer silica-zirconia-coated quartz glass samples. The single-layer AR-coated glass shows maximum transmittance with broad wavelength region. The AR coatings show relatively high mechanical strength, environmental stability, and relatively high LIDT values. The coated quartz glass optics could be used in the fabrication of Nd:phosphate laser.

2. Experimental

2.1 *Materials*

Heraeus made Suprasil 2 Grade B quartz glass, tetraethyl orthosilicate (TEOS, 99.0%; Aldrich), ammonia solution (NH_4OH, 25%; Merck), absolute ethanol (EtOH, Merck), hydrochloric acid (HCl, 37%; Merck), zirconyl oxychloride octahydrate (ZOO, 99.9%; Alfa Aesar), acetic acid (AcOH, 100%; Merck), zirconium (IV) propoxide (ZrP, ~70% in propanol; Fluka), acetylacetone (acac, extrapure AR; SRL), 1-propanol (Merck, 99%) and 2-butanol (Merck, 99%) have been used as-received without their further purifications.

2.2 *Preparation of sols*

To prepare single-(1LD) and multi-layer (2LD, 3LD) AR coatings on quartz glass, four types of precursor sols have been prepared. These are named as CS-1, PS-2, ZOS-3 and ZPS-4. In this respect, the silica sols are denoted as CS-1 and PS-2 that have been prepared with different compositions from TEOS. The CS-1 sol has a 9:1 (w/w) mixture of Sol A and Sol B, respectively, where the Sol A has been prepared with the composition, TEOS:NH_4OH:H_2O:EtOH of 1:0.1:3:40 (molar ratio) via conventional Stöber method [25]. In the composition of Sol B, TEOS:HCl:H_2O:EtOH is 1:0.005:4:27 (molar ratio). Sol B was a conventional acid-catalysed silica sol. The PS-2 sol has been prepared with w/w (2:8) mixture of Sol B and Sol C, respectively, where Sol C with the composition TEOS:NH_4OH:H_2O:EtOH of 1:0.05:3:40 (molar ratio) has been made via Stöber method. Two mixed zirconia-silica sols with 4 wt% equivalent metal oxide content have also been prepared from different precursors. One of the sols is denoted as ZOS-3 having the molar composition ZOO:TEOS:H_2O:AcOH:EtOH:2-ButOH of 1:0.1:10:2:39.4:10.5. In this sol preparation, the molar composition ZrP:TEOS:H_2O:HCl:acac:1-propanol:2-ButOH of ZPS-4 is 1:0.1:2:0.001:0.7:17.6:11.4.

2.3 *Deposition of coatings*

The quartz glass substrates have been cleaned following a standard cleaning procedure as reported in our previous work [26]. In a brief process, the substrates have been cleaned initially with soap water, then with tap water and distilled water followed by 30 min dipping in acetone-ethanol mixture under ultra-sonication. Finally, the washed samples have been dried by hot air. In case of single-layer deposition by dipping technique, the precursor sol has been aged for 24 h before the coating deposition. Using CS-1 sol, two overlay coatings have been applied at a fixed withdrawal speed of 9.2 cm min^{-1} to achieve the desired physical thickness of the coating layer. The coated films have been finally cured at 450°C for 30 min duration. Multi-

layer coatings have also been fabricated by stacking of the layers. The double-layer coating design consists of the layers from one ZPS-4 sol and two consecutive layers of PS-2 sol. The ZPS-4 sol has been used to deposit the coating with 16 cm min^{-1} withdrawal speed, but in case of PS-2 sol, the withdrawal speed for deposition was 22.3 cm min^{-1} and the curing temperature was 450°C for 30 min in air atmosphere. In case of triple-layer design, three consecutive layers have been deposited onto the glass substrate from ZOS-3, ZPS-4 and CS-1 sols. For this deposition, the first layer from ZOS-3 sol, the withdrawal speeds of 4.5 and 16 cm min^{-1} and 20 cm min^{-1} have been maintained for the fabrication of 1st, 2nd and 3rd layers, respectively. Initially, each consecutive layer was baked at 250°C and finally, cured at 450°C for 30 min in an air oven.

3. Characterizations

3.1 *Material properties*

Crystallinity/crystal phase of the metal oxide coatings have been examined by Grazing Incidence X-ray diffraction (GIXRD) study, where Rigaku Smart Lab, Japan make diffraction unit employing CuK_α radiation (1.5406 Å) operating at 9 kW in the diffraction angle range (2θ) of 10° to 80° has been employed. The particles dispersed in the sols have been analysed by measuring their sizes using a Malvern Zetasizer Nano ZS instrument (model no. ZEN3690). Surface morphology of the coatings has been analysed by an atomic force microscope (AFM, Nanosurf Easy Scan 2, Switzerland). The generated AFM data has been processed through WSxM 5.0 Develop 7.0-Image Browser software to calculate root mean square surface roughness (RMSSR) values keeping the area of measurement fixed to 50μm × 50μm. On the other hand, microstructural and elemental analysis of single-and multi-layer-coated samples have been performed by field emission scanning electron microscope (FESEM) and FESEM-EDS (ZEISS, SUPRA^{TM} 35VP), respectively. Scratch resistance of the coatings has also been measured according to ISO 15184 standard using Pencil Hardness Tester (Elcometer 501). This test is a constant-load scratch test. Pencil leads of different hardness grades (9B–9H) as the scratch stylus have been used. The same normal load with indenters of different hardness has been applied over the samples. The hardest pencil grade that did not cause any damage to the coated specimen has been considered as the hardness of the coating.

3.2 *Optical and textural properties*

Refractive index and physical thickness of the coatings have been measured from ellipsometric study. The dispersion curves (supplementary figure S1a) show the relation of RI *vs.* wavelength in the range 350–1000 nm. To compare with the experimental data of film physical thickness, theoretical simulation (table 1) has also been performed. The transmittance spectra of AR-coated single- and multi-layer samples have been measured by JASCO (V-730) make UV–Vis–NIR spectrophotometer in the wavelength range of 190–1100 nm. Optical constants like thickness and RI have been measured using J.A. Woollam (WVASE32, M-2000V) make ellipsometer varying incident angles. Optical quality of the coatings has been analysed from the degree of fitting of the measured curve with the calculated curve by Cauchy dispersion method. After fitting the curves, the thickness and RI @ 1054 nm value has been taken at the lowest reachable root mean square (RMS) value. LIDT value of the coated optics has been measured using a setup that consists of a pump laser (pulsed Nd:YAG laser, QT DNA, M/s Quanta systems), which can deliver maximum 1 J per pulse with 1–10 Hz repetition rate at 1064 nm with typical 7 ns pulse width. Beam profile of pump laser has been smoothened with suitable homemade vacuum spatial filter. This filtered and collimated pump laser radiation have been incident on target optics surface using a focusing lens L1 (f = 30 cm). Simultaneously, the laser energy, beam profile and pulse width have also been measured. Same spot has been radiated by 10 laser shots at 1 Hz repetition rate. A laser beam has been directed towards the optics at different locations and the optics has been observed carefully for any damage under Nomarsky microscope with 5x magnification. If damage is not found, the energy/power has been increased. The exercise has been repeated at ten other new locations. This process has been continued until any damage is observed by a visible spark or under the microscope. Damage threshold is then assigned to the highest energy/

Table 1. Optical designs of coatings modelled by TFCalc^{TM} software.

No. of layer(s)	Design	Physical thickness (nm)	Transmission @ 1054 nm (%)	Bandwidth >99% (nm)
Single-layer	1L	219.8	99.99	550
Bi-layer	0.71M	108.9	99.99	180
	1.13A	210.5		
Tri-layer	0.28H	39.4	99.95	275
	1.65M	250.9		
	1.03L	225.9		

power that optics can withstand without the laser causing damage.

4. Results and discussion

4.1 *Precursor sols*

In this work, two types of silica sols of 3 wt% silica content have been prepared from TEOS as a precursor material. starting from the precursor material TEOS. To prepare CS-1 and PS-2 sols, two factors have been varied to obtain different RI values. It is to be noted that CS-1 and PS-2 sols derived coatings show RI values of 1.19 and 1.42, respectively (supplementary figure S1a). Accordingly, these are denoted as n_L and n_A. Both the sols are the mixture of acid- and base-catalysed silica sol but the ratio of these sols is different. Also, in the base-catalysed sol, ammonia (NH_3) added for silica particle formation is not same. To prepare CS-1 sol, higher amount of NH_3 has been added compared to PS-2 sol. With increasing base content in the sol, larger size of colloidal silica particles is found to be generated [27]. Addition of higher amount of acid-catalysed silica, as in the case of PS-2 sol, fills out the pores in silica particles matrix, resulting in an increase of RI [28]. These two factors together explain the different RI of the coatings produced from these sols. To verify this fact, the size of the particles dispersed in sols has been measured by dynamic light scattering method. The particle size distribution curve (supplementary figure S1b) of CS-1 sol shows the size of dispersed colloidal particle in the range of 20–120 nm and majority are in the range of 45–60 nm. However, the majority of particles in PS-2 sol have the diameter of 39 nm (supplementary figure S1b). This data supports the effect of ammonia content added in the precursor sols.

For the hybrid zirconia-silica sols, namely ZOS-3 and ZPS-4; ZOO and ZrP have been chosen as the precursors, respectively. The choice of different precursors for these sols can be explained on the basis of producing different RI values towards the requirement. It is seen that ZOO-based sol-derived coating when annealed at 450°C forms crystalline layer (discussed later in section 4.3), but ZrP sol-derived coating does not crystallize at the same condition. It is noteworthy that crystalline coatings give high RI than amorphous ones as they are ordered in nature and have high mass density [29,30]. Also, the crystalline layer having high surface roughness (discussed later) helps better stacking of the next ZrO_2–SiO_2 layer in 3LD sample, which is supposed to be thicker film ($\sim$250 nm). The RI of ZOS-3 sol- and ZPS-4 sol-derived thin films exhibited RIs of 1.86 (n_H) and 1.74 (n_M), respectively (supplementary figure S1a). The particles dispersed in ZOS-3 (supplementary figure S2a) and ZPS-4 (supplementary figure S2b) sols are found to have a higher diameter (250–400 nm).

The RI values of the sols-derived coatings have been obtained from ellipsometric measurement and these are plotted to obtain dispersion curves (supplementary figure S1a).

4.2 *Optical designs of the coatings*

Single-layer AR coating has been designed according to standard quarter wavelength optical thickness phenomenon. Hence, it is easier to deduce the exact details by simple calculation. However, for multi-layer coating designs, manual calculation is found to be very complex in manner. Hence, computer-based designs have been adopted for the present work. In this respect, the bi-layer and tri-layer coating designs have been developed by TFCalc^{TM} software. It is to be noted that the calculations of this software are primarily based on [4×4] matrix formulation [24]. Using the RI of the developed films as the data set, the physical thickness of each layer has been optimized to get $\sim$100% transmittance at 1054 nm (table 1). For this simulation, the silica glass having RI = 1.46 has been used as substrate and air as incident and exit medium with unit RI. In table 1, the physical thickness of the single-layer design has been derived from equation (1).

$$1\mathrm{L} = n_L \times d = \lambda/4, \tag{1}$$

where λ = wavelength (1054 nm) and d = physical thickness.

In the similar manner, for bi-layer system, the thickness of the bottom layer has been derived from equation (2).

$$0.71\mathrm{M} = n_M \times d = \lambda/4 \tag{2}$$

All of the other layer thicknesses have been determined adopting the same method. In the multi-layer systems, quarter wavelength optical thickness rule has not been followed and hence, the non-unit quotients before the RI value have been determined by the software to obtain maximum transmittance at 1054 nm.

The bandwidth of highest transmission value is found to be of 550 nm for the single-layer design while for 3LD, it is 275 nm. The simulated bandwidth of maximum transmission value for the bi-layer system is the lowest and for this reason, the 2LD coating may also be called as V-shaped coating.

The physical thickness values obtained from table 1 are required to match the experimental result with simulated optical performances. Hence, all the synthesized sols have been coated on silicon wafer at varied withdrawal speed of dip coater. Film physical thickness has been obtained from ellipsometric measurement and the obtained data have been plotted as calibration curves (supplementary figure S3a–d). The supplementary figure S3a–d shows that the film physical thickness increases with increasing the withdrawal speed during the dip coating.

In some cases, single coat application is not enough to obtain the desired film thickness and hence, one or two more coats have been applied. It is to be noted that the

desired film physical thickness values of 118, 125, 40 and 105 nm, from CS-1 (supplementary figure S3a), PS-2 (supplementary figure S3b), ZOS-3 (supplementary figure S3c) and ZPS-4 (supplementary figure S3d) precursor sols derived films have been obtained at the withdrawal speeds of 4.5, 16, 9.2 and 22.3 cm min^{-1}, respectively. The respective withdrawal speed of each layer and other important parameters are tabulated in supplementary table S1.

4.3 *Phase structure of the coated samples*

Figure 1 shows the XRD patterns of AR-coated quartz glass. In this figure, the first layer coated with zirconia-silica shows sharp XRD peaks of tetragonal ZrO_2 and one very broad peak centred at 2θ (in degree), 21.2° for amorphous SiO_2 present in the film matrix as well as in the substrate [31]. The XRD peaks with the 2θ values observed at ~30.4°, ~35°, ~51° and ~62° correspond to tetragonal zirconia (JCPDS Card No. 80-0965) with the crystal planes (101), (110), (200) and (211), respectively. In this respect, Bumajdad *et al* [32] showed that the stability of cubic and tetragonal phases of ZrO_2 is dependent upon the crystallite size. Thus, for a particular crystal phase of ZrO_2, the crystallite size is important [32]. Hence, the crystallite size (D) of the generated tetragonal ZrO_2 particles has been calculated using Scherrer's equation (3).

$$D = k\lambda/\beta\cos\theta, \tag{3}$$

where k is the Scherrer's constant (0.89), λ is the wavelength of X-ray beam used (1.5406 Å), β is full-width at half-maxima (FWHM) taken for all the major peaks and θ is the diffraction angle.

From equation (3), the average crystalline size is found to be 9.4 nm. It is to be further noted that the cubic ZrO_2 could only be stabilized when the particle size is small (below 6 nm) and monoclinic ZrO_2 particles would be formed at >20 nm [32]. Therefore, the size of the crystals is found to be a favourable factor for the formation of tetragonal phase of ZrO_2 [32]. The XRD pattern of second layer (zirconia-silica) coating derived from zirconium (IV) propoxide shows amorphous behavior and also the third-layer porous silica-coated film is similar in nature.

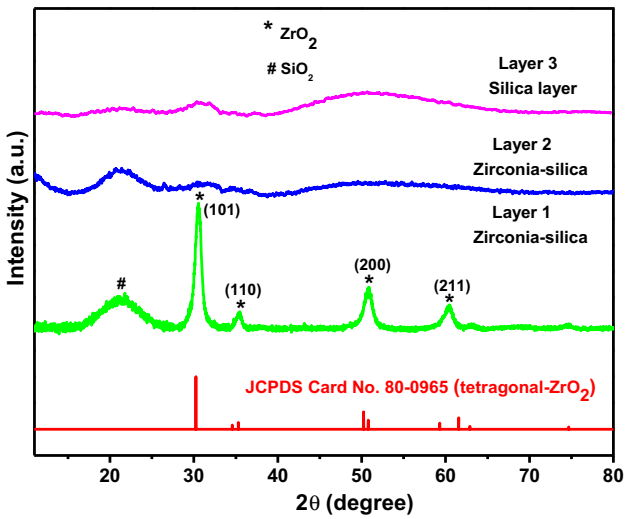

Figure 1. X-ray diffraction patterns of AR-coated quartz glass samples.

4.4 *Physical thickness and surface morphology of the coatings*

Most crucial part of an AR coating is to control the physical thickness of each layer as per theoretical simulation to get highest optical transmittance. By using ellipsometric data, the precursor sols for the coatings have been calibrated for their physical thickness against withdrawal speed of the dip coater. In this respect, ellipsometric measurement has been performed on single-layer films. To obtain actual coating thickness of each layer, cross-sectional FESEM of the developed films has been carried out. From figure 2a, the physical thickness of the single-layer coating has been calculated and it is 228 nm, which is close to the quarter wavelength thickness of 219.8 nm. This little deviation in thickness value could reduce optical transmittance (discussed in the next section). Figure $2a_1$ shows energy-dispersive X-ray (EDX) spectrum of single-layer coating to confirm the presence constituent elements in the coating. The cross-sectional image of the double-layer AR coating (figure 2b) clearly shows the formation of two distinctive layers, where the thickness of bottom zirconia-silica layer and top silica layer are found to be 195 and 155 nm, respectively. The top silica layer appears to be partially diffused into the bottom layer. Sol–gel coatings cured at low temperature are always somewhat porous in nature and hence, the diffusion between two layers could be possible. An elemental mapping of different constituent elements is also taken from the cross-sectional FESEM of the coating area in each layer (figure $2b_1$). The elemental mapping curve shows increasing concentration of zirconium in bottom layer and a rise in the silicon curve for bottom layer. The substrate and coating can be differentiated by the absence of oxygen. The EDX spectra for double layer coating are shown in figure $2b_2$. The cross-sectional FESEM view of triple-layer coating clearly shows the presence of three layers distinctively (figure 2c). From the cross-sectional FESEM image, the thickness of three layers in the triple-layer coating has been calculated to be 50, 240 and 100 nm for 1st layer, 2nd layer and 3rd layer, respectively. In case of zirconia-silica coating layer, the desired film thickness has been achieved easily, but the thickness of silica layer (3rd layer) is found to be low. On the other hand, the elemental composition of the triple-layer coating is confirmed from FESEM elemental mapping curve (figure $2c_1$) and EDX spectra (figure $2c_2$).

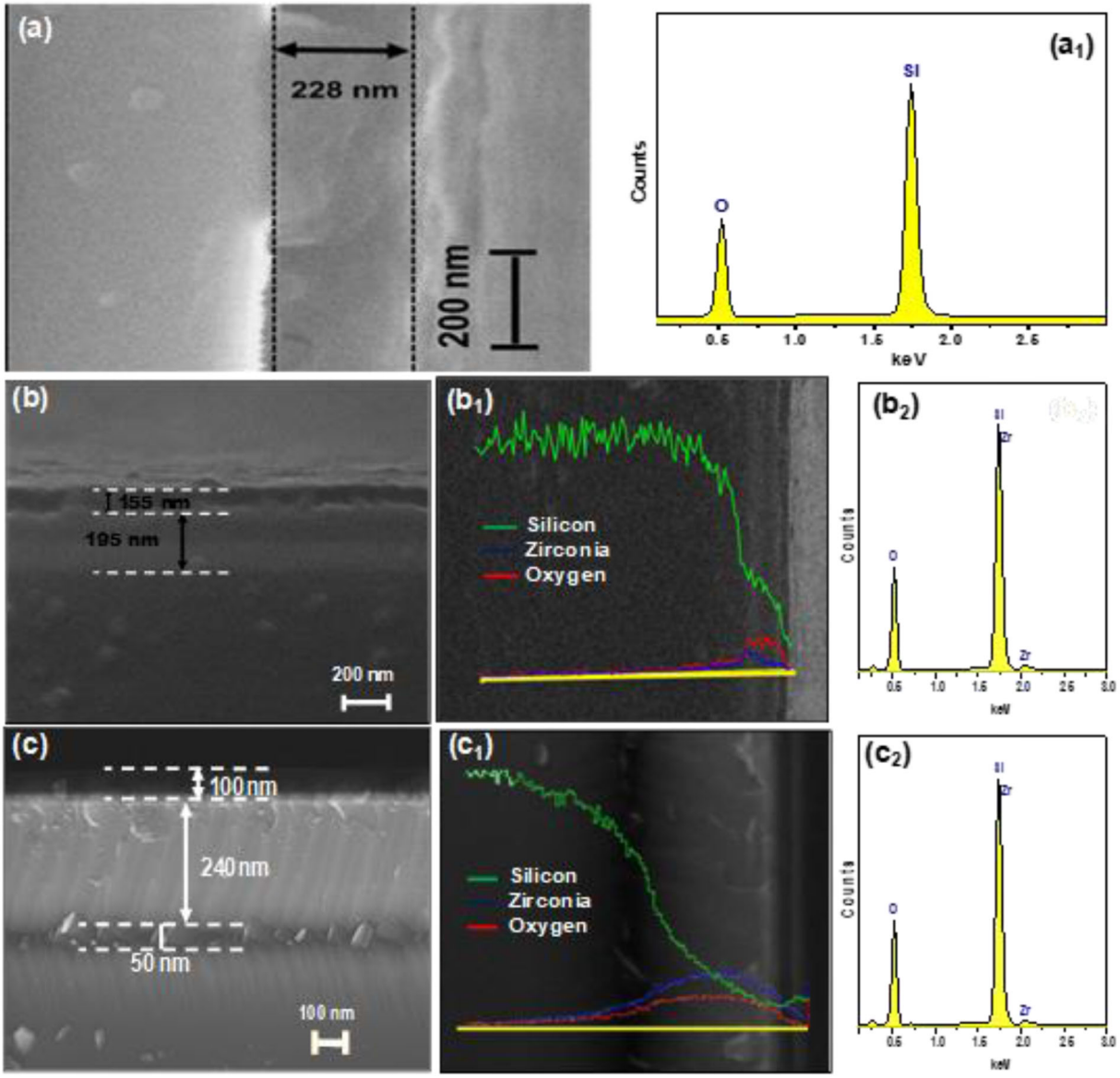

Figure 2. (**a**) Cross-sectional FESEM image of single-layer AR coating; (**a$_1$**) EDX spectra of the coating obtained from **a**; (**b**) cross-sectional FESEM image, (**b$_1$**) elemental mapping of double-layer AR coating obtained from **b**. (**b$_2$**) EDX spectra of the coating. (**c**) Cross-sectional FESEM image, (**c$_1$**) elemental mapping of triple-layer AR coating and (**c$_2$**) EDX spectra of the coating obtained from **c**.

The FESEM study has also been performed to observe the surface morphology of coated samples. The FESEM images have been taken after each layer of the coating deposition and the curing for a multi-layer film subsequently. All the films have been deposited on Si-wafer in a similar manner as done on glass substrate for the FESEM study. The AFM images have also been obtained from the coatings on Si-wafer. The RMSSR values have been calculated after analysing the images. Therefore, each layer of multi-layer-coated sample has been analysed with the help of AFM and FESEM studies. The FESEM image shows the formation of spherical silica particles (figure 3a) in single-layer coating on wafer, and the AFM image (figure 3a$_1$) also reveals a rough surface with an average surface roughness value of 9.68 nm. The AFM image (figure 3b) of bottom layer of 2LD sample exhibits a smooth surface with a roughness value of 8.5 nm. The FESEM image also shows a smooth surface. The FESEM image (figure 3c) of the final layer also shows the formation of silica particle, but the particle formation is seemed to be denser than the single-layer silica coating (figure 3a). This explains the silica layer with higher RI as obtained from PS-2 precursor sol. AFM image (figure 3c$_1$) of this layer shows RMSSR value of 11.8 nm. First layer (figure 3d) of the 3LD sample image shows a roughness of 18 nm. This high surface roughness value could be attributed to the crystalline nature (figure 1) of the

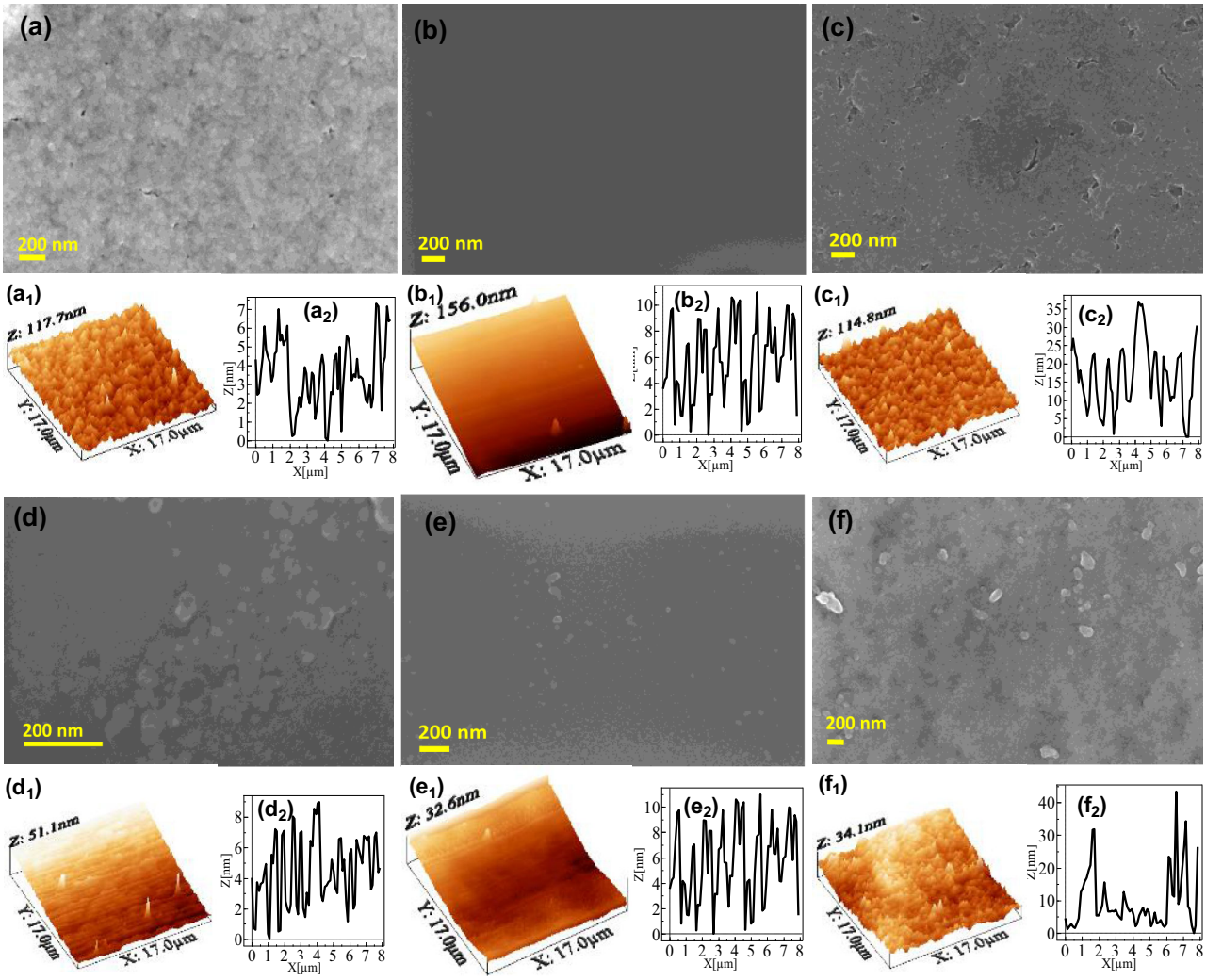

Figure 3. FESEM (**a**, **b**, **c**, **d**, **e**, **f**) and 3D AFM images ($\mathbf{a_1}$, $\mathbf{b_1}$, $\mathbf{c_1}$, $\mathbf{d_1}$, $\mathbf{e_1}$, $\mathbf{f_1}$) with their corresponding line scan profiles ($\mathbf{a_2}$, $\mathbf{b_2}$, $\mathbf{c_2}$, $\mathbf{d_2}$, $\mathbf{e_2}$, $\mathbf{f_2}$) of the AR-coated quartz glass samples with different coated layers. (**a**, $\mathbf{a_1}$, $\mathbf{a_2}$) single layer (1LD) AR coating; (**b**, $\mathbf{b_1}$, $\mathbf{b_2}$) 1st layer of double-layer (2LD) AR coating; (**c**, $\mathbf{c_1}$, $\mathbf{c_2}$) 2nd layer of double-layer AR (2LD) coating; (**d**, $\mathbf{d_1}$, $\mathbf{d_2}$) 1st layer of triple-layer (3LD) AR coating; (**e**, $\mathbf{e_1}$, $\mathbf{e_2}$) 2nd layer of triple-layer (3LD) AR coating; (**f**, $\mathbf{f_1}$, $\mathbf{f_2}$) 3rd layer of triple-layer (3LD) AR coating.

film. Second layer of ZPS-4 sol-derived 3LD AR coating shows (figure 3e) a smooth surface with the formation of few particles. On the other hand, the AFM image (figure 3e_1) also shows a smooth surface and the measured RMSSR value is 5.7 nm. The FESEM image of the top most layer of silica coating (figure 3f) shows a rough texture due to generation of spherical silica particles. The formation of silica particles is also supported by FESEM and AFM analyses (figure 3f and f_1). It is found that the RMSSR surface roughness of 3rd layer silica coating is 16.42 nm.

4.5 *Transmittance spectra of the samples*

Single and multi-layer AR-coated film samples have been subjected to transmittance spectral study to find out the percentage of light transmitted through the coatings, particularly in near-infrared region. The single-layer-coated film shows ∼99% transmittance, while double- and triple-layer-coated films show ∼ 98.1 and ∼ 97.6%, respectively, at 1054 nm. The fringes observed in the transmission spectra (figure 4a) appeared due to spontaneous interference between reflection of light between air-film interface and film-substrate interface [33]. This explains the occurrence of more fringes in multi-layer transmission curves due to increase in number of interfaces [33]. Moreover, the single-layer designed AR effect could be seen for a broad wavelength range, whereas the multi-layer AR effect is seen in more specific narrower wavelength range.

A gradual decrease in transmittance values and increasing deviation from the calculated values have been observed with increase in number of coating layers. For single-layer system, the deviation of coating thickness was found to be less. Hence, lesser loss in transmittance is obtained. For multi-layer systems, the deviations are found to be

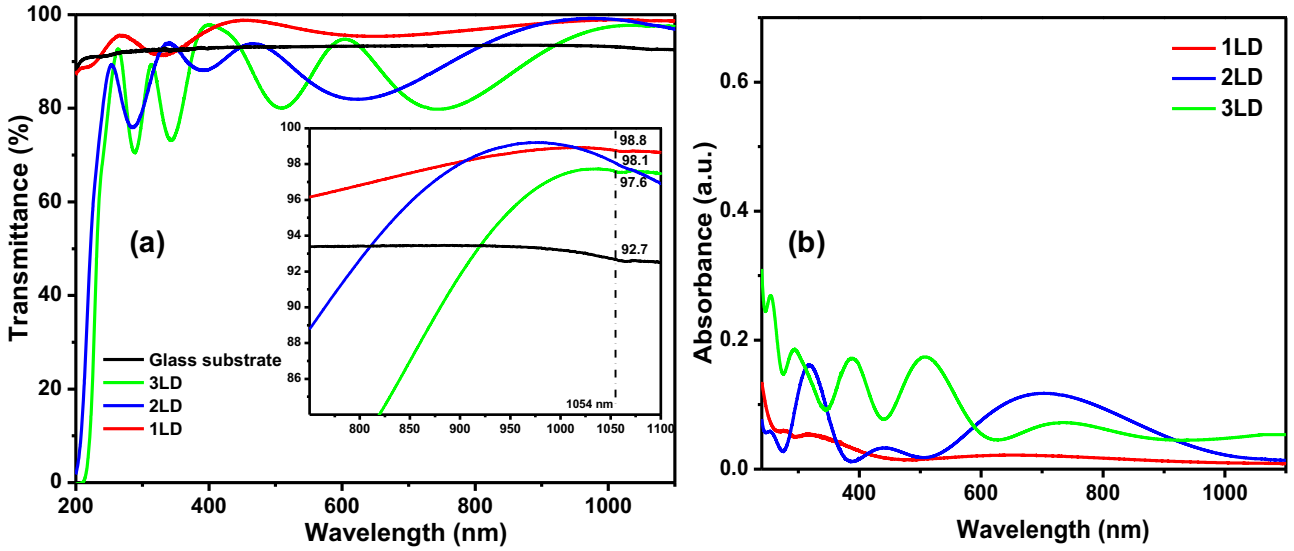

Figure 4. (**a**) UV–visible transmittance and (**b**) absorbance spectra of AR-coated samples on quartz glass (inset of **a** shows the percentage of transmission values at 1054 nm).

enhanced and therefore, the amount of loss in transmittance is found to be increased. A scattering loss in multi-layer-coated samples could also result in transmittance loss. Based on vector scattering theory, equation (4) having the relation with total scattering loss (TS) in transmittance and RMS surface roughness (σ) is reported [34].

$$\mathrm{TS} = R_0(4\pi\sigma/\lambda)^2, \tag{4}$$

where R_0 is Fresnel reflection of the surface, λ is the wavelength.

Fresnel reflection, R_0 is given by equation (5).

$$R_0 = \left(\frac{n_t - n_i}{n_t + n_i}\right)^2, \tag{5}$$

where, n_t (quartz glass) = 1.46 and n_i (air) = 1.

From equation (5), R_0 of the quartz glass is found to be 3.37%. The RMSSR values (σ) of developed samples have been obtained from the AFM analysis (section 4.4). From equation (4), for single-layer AR-coated sample (1LD), the TS is found to be 0.045% using σ-value of 4.68 nm. In a similar manner, the TS for 2LD sample is found to be 0.06%, when σ = 11.8 nm, whereas the TS for 3LD sample is 0.13% when σ = 16.42 nm. The scattering loss calculated for each sample shows an increasing trend with RMS surface roughness value of the coated surface. The scattered light from rough surface would get trapped in the film by total internal reflection and thus, the scattering could cause an increased absorption [35]. In this respect, the absorption spectra of the final samples (figure 4b) show minimum absorbtion for the 1LD specimen, which increased gradually with increasing the number of layers in multi-layer samples. This result mostly coincides with the transmittance values at 1054 nm.

4.6 *Measurement of LIDT of the coatings*

The LIDT values have been measured using a 1064 nm laser of 7 ns pulse width and 0.7 mm^2 laser beam spot area. The LIDT values are given in table 2. Single-layer AR coating shows relatively high LIDT value compared to multi-layer coatings, and from double layer to triple layer a consecutive decrease in LIDT values is found.

Laser damage probability (p) of a thin film surface is given by,

$$p = n/N, \tag{6}$$

where n is damaged zones and N is total no. of tested zones. It is known that the LIDT value obtained for the targeted sample depends upon this probability of laser damage of surface. This probability mostly depends on the coating quality, which may be expressed with the term surface density of defects (d_s). These defects, which may be caused due to environmental particle entrapment, pit formation, and presence of cracks or scratches in the coating matrix, have higher energy density than the intrinsic damage

Table 2. Measurement condition and LIDT values of the AR coated samples.

Sample ID	Measurement condition	Test mode	LIDT (J cm^{-2})
1LD	Laser:pulsed Nd:YAG laser with pulse width −7 ns Test environment: Ambient atmosphere	10-on-1	8.7
2LD		10-on-1	4.6
3LD		10-on-1	2.4

threshold of the coating materials. Hence, these spots get damaged at lower laser fluence. According to the work of Natoli *et al* [36], the damage probability and surface defects are related to equation (7).

$$\ln(1-p) = \frac{Sd_s}{2}(\ln T - \ln F), \tag{7}$$

where S = defect spot size, T = damage threshold value, F = fluence maximum.

From equation (7), it is implied that with increasing S and d_s value, p will increase and hence, the LIDT value of the coating is found to be decreased. This argument explains that the single-layer SiO_2 AR-coating LIDT value is lesser than intrinsic value of SiO_2 as material. For multi-layer AR coating as thickness increases, bulk defects also play a key factor in laser damage. This factor could be introduced as bulk defect density (d_v) in equation (7). These two densities can be related as, $d_s = d_v \times e$, where e = coating physical thickness. Therefore, equation (7) becomes,

$$\ln(1-p) = \frac{Sd_v e}{2}(\ln T - \ln F). \tag{8}$$

From the above relation, it is concluded that, a higher physical thickness means higher damage probability and lesser LIDT value (T), as p and T are inversely related. Hence, the decrease in T-values of 2LD and 3LD AR coatings could be justified on the above basis.

Other than the physical thickness, another criterion that contributes to the decrease in LIDT value of 3LD coating is the internal stress generated in the film based on crystallinity and crystallite size of the zirconia-silica layer (figure 1). It is known that the LIDT value is inversely proportional to the generated film internal stress. The thin film that is annealed at a relatively lower temperature (below 500°C) is found to be poorly crystalline/semicrystalline in nature, may generate higher stress resulting reduced LIDT value [37]. Also, smaller crystallite size (9.4 nm, refer to section 4.3) of the ZrO_2 crystals is observed, which indicates higher strain generation in the coating. This is because the smaller crystallite size may develop greater number of grain boundaries, causing an enhancement of internal stress [38]. These factors together may explain the increased internal stress vis-à-vis the decrease in LIDT value of 3LD sample compared to 2LD coating.

In addition to the LIDT measurement, the morphology of the damaged coating has also been observed with differential interference contrast microscope to understand the type of damage occurred on the coating surface. Comparing between the damaged and undamaged images (figure 5), it is clear that the damages are found to be initiated from the defect points of the coating surface. If the defects are less, the LIDT value is increased. Single layer (figure 5a and a_1), double layer (figure 5b and b_1) and triple layer (figure 5c and c_1) coated surfaces are found to be damaged under the laser radiation. It is known that in optics, the surface damage caused by laser irradiation can be occurred through

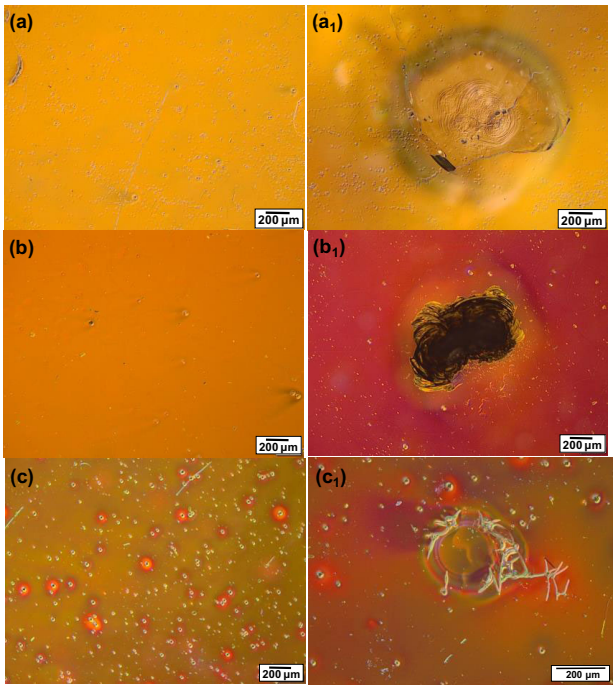

Figure 5. Optical microscope images showing the surface morphologies of undamaged and damaged single-layer (**a**, **a$_1$**), double-layer (**b**, **b$_1$**) and triple-layer (**c**, **c$_1$**) AR-coated quartz glass samples after laser beam irradiations.

various type of mechanisms. These mechanisms depend largely on the pulse duration of the laser used. In this study, the pulsed laser setup used had a pulse width of 7 ns. It is to be noted that the damage from nanosecond-ordered pulse duration occurs through thermal effects, dielectric breakdown, carrier–carrier scattering and carrier phonon scattering [39]. In case of thermal effect, the energy from laser pulses gets absorbed by materials in the film matrix causing heat diffusion and distortion. On the other hand, dielectric breakdown is also caused by excess absorption of laser energy, which causes exceeding the materials breakdown voltage. Other mechanisms may also be initiated when electrons accelerated by electric field that collides with electrons or phonons and scattered them. However, the damage morphologies that are observed (figure 5) in the samples could have been created via following one or more mechanisms. Therefore, in the present work, it is hard to identify the exact reason/(s) associated with a particular morphology of the damage of the coatings.

4.7 *Pencil hardness and durability of the coatings*

Hardness is the resistance of a surface against scratching [40]. In this respect, the scratch-resistant coatings are easier to handle and has better application. Incorporation of ZrO_2 to AR coating gives them better durability against time (supplementary figure S4) with enhanced hardness. The

hardness of the coatings has been tested by pencil hardness scratch test. Single-layer AR coating shows 2B pencil hardness, i.e., when scratched with 2B pencil hardness no indentation mark is left on surface. In a similar manner, for triple-layer AR coating, after deposition of zirconia layers' pencil hardness is found to be 6H, but after applying final porous silica layer over the zirconia layers' pencil hardness reduced to B. For double-layer coating after applying semi-porous silica layer, the hardness is found to be 7H. The reason for such superior scratch resistance can be attributed to the semi-porous silica (RI $\sim$1.4) with better binding property. The filler [41] based on siloxane chains from acid-catalysed silica sol, forms Zr–O–Si linkage[42] with the underneath ZrO_2–SiO_2 layer. In case of 3LD, the amount of filler portion, i.e., acid-catalysed silica sol decreases, which does not facilitate the bonding between two layers. The porous silica coating with low RI (1.22) in case of triple-layer AR coating decreases the final coating hardness when applied on zirconia layers. All the AR-coated films show very good environmental stability when stored under ambient conditions. It is to be noted that after storing the sample for 1-year duration at room temperature, the AR-coated samples showed (supplementary figure S4) a decrease in transmittance value within 0.1–0.5%.

5. Conclusion

In conclusion, a single-layer silica AR coating on quartz glass ($\sim$99% transmittance) and bi-layer as well as tri-layer AR coatings with $\sim$98.1 and $\sim$97.6% transmittance, respectively, at 1054 nm have been fabricated by sol–gel dip-coating technique. Single-layer porous silica coating has been deposited from TEOS-derived precursor silica sol, whereas multi-layered coatings have been fabricated by stacking zirconia and silica layers as high index and low index materials, respectively. Zirconium oxychloride and zirconium *n*-propoxide have been used as precursors for zirconia layers. Using TFCalc^{TM} software, theoretical calculations have been done for the development of AR coatings. Finally, the AR coated samples have been tested for their tolerance of high power pulsed laser by measurement of their LIDT values. A single-layer AR coating on quartz glass shows high LIDT value, whereas the multi-layer AR coatings exhibit moderate LIDT values. The fabricated AR coating with high LIDT value could find application in Nd:phosphate high power laser system whereas the 2LD and 3LD systems could be useful for more wavelength-specific purposes.

Acknowledgements

This study has been done under the project (GAP0624) sponsored by the Department of Atomic Energy (DAE), Government of India (*vide* Sanction No. 34/14/09/2018-BRNS). We thankfully acknowledge the help rendered by Materials Characterization and Instrumentation Division of CSIR-CGCRI, Kolkata for XRD, particle size distribution and FESEM characterizations.

References

[1] Biswas P K 2011 *J. Sol-Gel Sci. Technol.* **59** 456
[2] Moayedfar M and Assadi M K 2018 *Rev. Adv. Mater. Sci.* **53** 187
[3] Schirone L, Sotgiu G and Califano F P 1997 *Thin Solid Films* **297** 296
[4] Enger R C and Case S K 1983 *Appl. Opt.* **22** 3220
[5] Chen Y W, Han P Y and Zhang X C 2009 *Appl. Phys. Lett.* **94** 041106
[6] Papet P, Nichiporuk O, Kaminski A, Rozier Y, Kraiem J, Lelievre J F *et al* 2006 *Sol. Energy Mater Sol. Cells* **90** 2319
[7] Thomas I M 1997 *Proc. SPIE* **3136** 215
[8] Liu H, Jensen L, Ma P and Ristau D 2018 *Adv. Opt. Technol.* **7** 23
[9] Zhu M, Xing H, Chai Y, Yi K, Sun J, Wang J *et al* 2016 *Opt. Eng.* **56** 011003
[10] Park M S and Kim J K 2005 *Langmuir* **21** 11404
[11] Joo W, Park M S and Kim J K 2006 *Langmuir* **22** 7960
[12] Walheim S, Schaffer E, Mlynek J and Steiner U 1999 *Science* **283** 520
[13] Wang J, Hu W, Han W, Zhu Q and Xu Y 2018 *High Power Laser Sci. Eng.* **6** 26
[14] Liu X, Lu X, Wen P, Shu X and Chi F 2017 *Appl. Surf. Sci.* **420** 180
[15] Mazur M, Wojcieszak D, Domaradzki J, Kaczmarek D, Song S and Placido F 2013 *Opto-Electron Rev.* **21** 233
[16] Gil-Rostra J, García-García F J, Yubero F and González-Elipe A R 2014 *Sol. Energy Mater. Sol. Cells* **123** 130
[17] Sabnis R W, Guerrero D J, Brewer T and Spencer J 2005 US Patent No. 6,869,747
[18] Druzhinin A, Ostrovskii I, Yerokhov V, Khoverko Y, Nichkalo S and Kogut I U 2012 *Proceedings of international conference on modern problem of radio engineering, telecommunications and computer science* p 484
[19] Eriksson T S and Granqvist C G 1983 *Appl. Opt.* **22** 3204
[20] Sun X W and Kwok H S 1999 *J. Appl. Phys.* **86** 408
[21] Deng C and Ki H 2016 *Sol. Energy Mater. Sol. Cells* **147** 37
[22] Martinet C, Paillard V, Gagnaire A and Joseph J 1997 *J. Non-Cryst. Solids* **216** 77
[23] Zhang S, Zhao X, Wang P, Xiao P, Luo J and Jiang B 2019 *J. Sol-Gel Sci. Technol.* **92** 598
[24] Ye L, Zhang X, Zhang Y, Li Y, Zheng W and Jian B 2016 *J. Sol-Gel Sci. Technol.* **80** 1
[25] Stöber W, Fink A and Bohn E 1968 *J. Colloid Interface Sci.* **26** 62
[26] Khan H, Samanta S, Seth M and Jana S 2020 *J. Mater. Sci.* **94** 141
[27] Park S K, Kim K D and Kim H T 2002 *Colloids Surf. A: Physicochem. Eng. Asp.* **197** 7
[28] Thomas I M 1992 *Appl. Opt.* **31** 6145

[29] Ghazaryan L, Handa S, Schmitt P, Beladiya V, Roddatis V, Tünnermann A *et al* 2021 *Nanotechnol.* **32** 095709
[30] Jerman M, Qiao Z and Mergel D 2005 *Appl. Opt.* **44** 3006
[31] Musić S, Vinceković N F and Sekovanić L 2011 *Braz. J. Chem. Eng.* **28** 89
[32] Bumajdad A, Nazeer A A, Sagheer F A, Nahar S and Zaki M I 2018 *Sci. Rep.* **8** 3695
[33] Sunke V, Bukke G N and Suda U 2018 *J. Nanomed. Res.* **7** 65
[34] Trost M 2015 *PhD Thesis* (Friedrich-Schiller-Universität Jena)
[35] Khan H, Seth M, Samanta S and Jana S 2020 *J. Sol-Gel Sci. Technol.* **94** 141
[36] Natoli J Y, Gallais L, Akhouayri H and Amra C 2002 *Appl. Opt.* **41** 3156
[37] Wang X, Wu G, Zhou B and Shen J 2012 *Opt. Express.* **20** 24482
[38] Balogh-Michels Z, Stevanovic I, Borzi A, Bächli A, Schachtler A, Gischkat T *et al* 2021 *J. Eur. Opt. Soc.: Rapid Publ.* **17** 3
[39] Chambonneau M, Rullier J, Grua P and Lamaignère L 2018 *Opt. Express.* **26** 21819
[40] Whitney D L, Fayon A K, Broz M E and Cook R F *J. Geosci. Educ.* **55** 56
[41] Rodrıguez H A and Casanova H 2018 *Hindawi J. Nanotech.* Article ID 7589051 doi https://doi.org/10.1155/2018/7589051
[42] Carnegie M R, Sherine A, Sivagami D and Sakthivel S 2016 *J. Sol-Gel Sci. Technol.* **78** 176